International Journal of Minerals, Metallurgy and Materials
Volume 28, Number 12, December 2021, Page 1966
https://doi.org/10.1007/s12613-020-2123-z

Microstructure evolution and mechanical properties of Mg–9Al–1Si–1SiC composites processed by multi-pass equal-channel angular pressing at various temperatures

Xiang-peng Zhang[1)], *Hong-xia Wang*[1,2)], *Li-ping Bian*[1)], *Shao-xiong Zhang*[1)], *Yong-peng Zhuang*[1)], *Wei-li Cheng*[1)], *and Wei Liang*[1,2)]

1) Shanxi Key Laboratory of Advanced Magnesium based Materials, College of Materials Science and Engineering, Taiyuan University of Technology, Taiyuan 030024, China

2) Key Laboratory of Interface Science and Engineering in Advanced Materials, Ministry of Education, Taiyuan University of Technology, Taiyuan 030024, China

(Received: 21 April 2020; revised: 30 May 2020; accepted: 17 June 2020)

Abstract: In this study, Mg–9Al–1Si–1SiC (wt%) composites were processed by multi-pass equal-channel angular pressing (ECAP) at various temperatures, and their microstructure evolution and strengthening mechanism were explored. Results showed that the as-cast microstructure was composed of an α-Mg matrix, discontinuous $Mg_{17}Al_{12}$ phase, and Chinese script-shaped Mg_2Si phase. After solution treatment, almost all of the $Mg_{17}Al_{12}$ phases were dissolved into the matrix, whereas the Mg_2Si phases were not. The subsequent multi-pass ECAP at different temperatures promoted the dynamic recrystallization and uniform distribution of the $Mg_{17}Al_{12}$ precipitates when compared with the multi-pass ECAP at a constant temperature. A large number of precipitates can effectively improve the nucleation ratio of recrystallization through a particle-stimulated nucleation mechanism. In addition, the SiC nanoparticles were mainly distributed at grain boundaries, which effectively prevented dislocation movement. The excellent comprehensive mechanical properties can be attributed to grain boundary strengthening and Orowan strengthening.

Keywords: magnesium alloy; multi-temperature ECAP processing; Mg_2Si; mechanical property

1. Introduction

Magnesium alloy is a light metallic structural material owing to its low density, damping properties, and easy recycling. Thus, it has received considerable interest in the aerospace, automobile, 3C, and other manufacturing fields and has good prospects for advanced development [1–2]. However, the poor thermal stability and insufficient mechanical properties of Mg alloys restrict their large-scale applications in industrial production. Deformation, alloying, and composite formation are important methods to improve the microstructure and mechanical properties of Mg alloys [3–5]. Mg–Al–Si-based alloys may overcome the above disadvantages because Al exerts an excellent solid solution strengthening effect in Mg. In addition, alloying with Si can introduce a Mg_2Si phase with high melting point, which can significantly improve the thermal stability of the alloy [6–7]. However, the addition of Al and Si introduces coarse $Mg_{17}Al_{12}$ and Mg_2Si phases during casting, which splits the magnesium matrix and ultimately decreases the ductility of the material [8–9]. Recently, composites reinforced by SiC nanoparticles have attracted increasing attention because of their capacity to promote the grain refinement and fragmentation of $Mg_{17}Al_{12}$ and Mg_2Si phases, which can contribute to obtaining high-strength alloys [10–11].

However, SiC nanoparticles form clusters easily and are difficult to distribute uniformly in the α-Mg matrix during casting [12–13]. Grain refinement is an important method that can improve strength and ductility, but whether or not SiC nanoparticles promote grain refinement remains to be clarified. Severe plastic deformation is widely used to prepare ultrafine grains and modify the morphology and distribution of secondary phases; equal-channel angular pressing (ECAP) is a convenient method of deformation [14–16]. However, grain refinement is limited in traditional ECAP processing because the grain size is no longer refined or even

Corresponding author: Hong-xia Wang E-mail: wanghxia1217@163.com

increased beyond a certain number of extrusion passes [17–20]. Low deformation temperatures can promote the dynamic recrystallization and fragmentation of the bulk second phase, but low extrusion temperatures make the alloys difficult to deform or even crack [21]. Fine grains are difficult to obtain within limited ECAP passes. Nie *et al*. [8] reported that the average grain size of SiC_p/AZ91 after six passes (three passes at 400°C and three passes at 350°C) during multi-direction forging (MDF) at various temperatures is 5.3 μm, which is obviously finer than 18.5 μm after six passes of MDF at a constant temperature of 400°C. Consequently, the yield strength (YS) is improved to 210 MPa for multi-pass MDF at various temperatures compared with 190 MPa for MDF at a constant temperature. Therefore, multi-pass MDF at various temperatures is beneficial to obtaining fine grains and improving the mechanical properties of alloys. However, whether or not the multi-pass ECAP at various temperatures exerts similar effects on Mg–Al–Si-based alloys is unclear.

Therefore, to overcome the various disadvantages of Mg alloys, this study attempts to obtain excellent comprehensive mechanical properties of Mg–Al–Si by combining the multi-pass ECAP at various temperatures and adding SiC reinforcement nanoparticles. The relationship between microstructure evolution, texture, and mechanical properties of Mg–9Al–1Si–1SiC with multi-pass ECAP at various temperatures was systematically studied. Furthermore, the strengthening mechanism of the material was analyzed and discussed in detail. The proposed method may open a new path for improving the comprehensive mechanical properties of Mg alloys.

2. Experimental

An experimental alloy with a nominal composition of Mg–9Al–1Si–1SiC (wt%) was fabricated with Mg (purity 99.9wt%), Al (purity 99.99wt%), Al–30Si master alloy, and SiC nanoparticles with an average diameter of 60 nm. The mixture was melted in an electrical-resistance furnace in the presence of CO_2 and SF_6 protective gas to prevent oxidation. After pure Mg, Al, and Al–30Si master alloy were molten, the molten alloy was cooled to 590°C. Then, 1wt% SiC nanoparticles were added into the semi-solid alloy, and the melt was stirred for 10 min. The melt was rapidly reheated to 720°C and retained at this temperature for 30 min. Finally, the melt was poured into a cylindrical steel mold (inner diameter, 90 mm) that had been preheated at 200°C for 30 min. The as-cast sample was solution treated at 420°C for 24 h followed by water quenching. Before ECAP processing, the homogenized samples were preheated at the extrusion temperature for 30 min. Specimens with a gauge size of 12 mm × 12 mm × 55 mm were formed by extrusion through a modified ECAP die (φ = 90°, ψ = 16°) using Bc route, which means that samples were rotated 90 degrees in the same direction before next pass [22–23]. Up to four passes were completed at an average extrusion rate of 2 mm·min^{-1}, and the ECAP parameters are shown in Table 1.

Table 1. ECAP parameters of experimental alloys

Sample	First-pass temperature / °C	Second-pass temperature / °C	Third-pass temperature / °C	Fourth-pass temperature / °C
I	400	400	400	400
II	400	360	320	320
III	400	360	360	320
IV	400	400	320	320

The microstructure of the alloy before ECAP deformation was evaluated under an optical microscope. The morphology and distribution of the secondary phases and tensile fractures were observed through scanning electron microscopy (SEM). Phase analysis and elemental composition identification were performed using X-ray diffraction (XRD; TD-3500) and energy dispersive spectroscopy (EDS), respectively. Image-Pro Plus 6.0 software was used to calculate the average grain size and volume fraction of grains transformed by dynamic recrystallization (DRX) and dynamic precipitation. The texture of the ECAP samples was tested using the TD-3500 XRD instrument with Cu K_α radiation (wavelength λ = 0.15406 nm) at 45 kV and 40 mA and scanning angles from 0° to 70°. The SiC nanoparticles and dislocations were further characterized through transmission electron microscopy (TEM). Finally, uniaxial tensile tests were conducted on a DNS100 universal testing machine with a rate of 0.2 mm·min^{-1} at room temperature, and the tensile results were derived from the average of at least three valid tests.

3. Results and discussion

3.1. Microstructure characterization before ECAP

Figs. 1(a) and 1(b) show the optical micrographs of the as-cast and solution-treated samples, respectively. As shown in Fig. 1(a), the as-cast sample has a typical dendritic structure and the secondary phases are homogeneously distributed in the matrix. SEM micrographs of the as-cast and solution-treated samples are presented in Figs. 1(c) and 1(d) to show the morphology and distribution of the secondary phases. The microstructure of the as-cast sample consists of an α-Mg matrix (black region), eutectic phases (light gray region), and

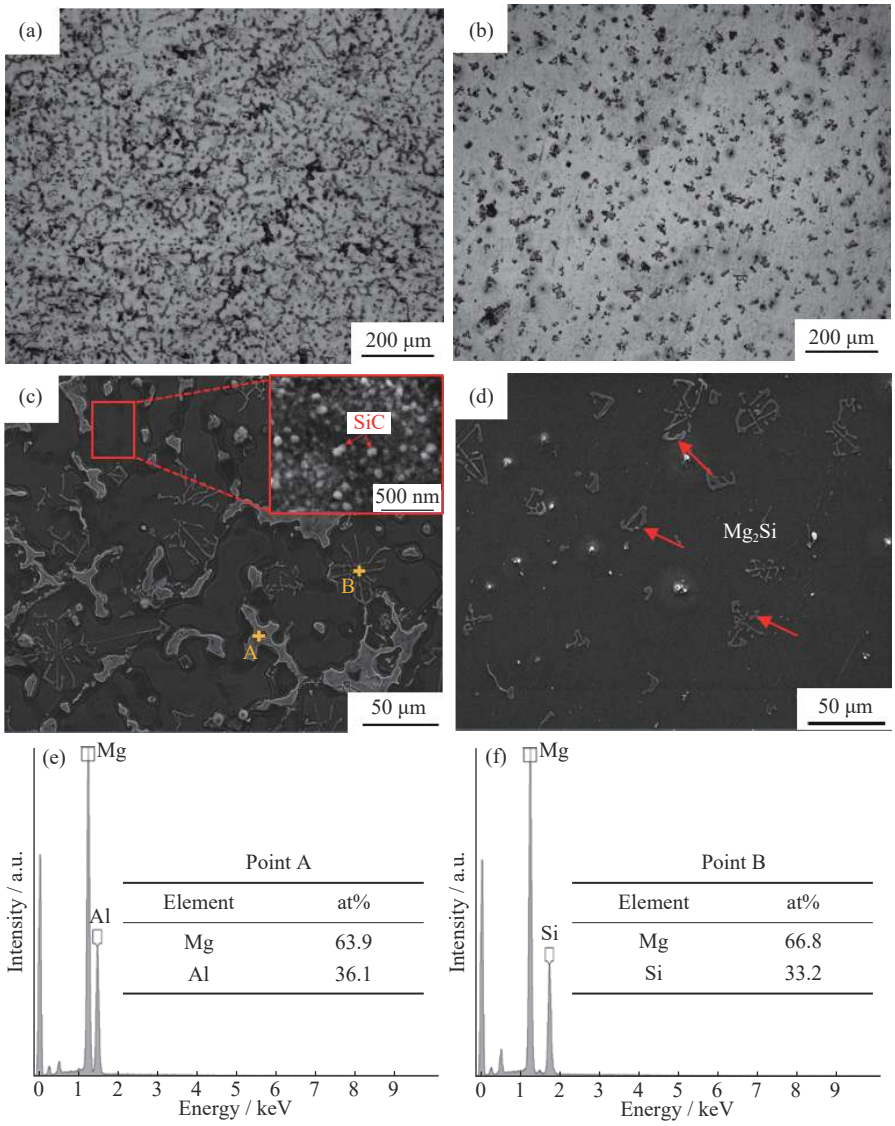

Fig. 1. Optical, SEM microstructure, and EDS results for samples: (a, c) as-cast composites; (b, d) solution-treated composites; (e, f) EDS results for points A and B in (c).

Chinese script-shaped phases (dark gray region). The eutectic phases are distributed mostly along the triangular grain boundaries with a discontinuous network morphology. EDS results are presented in Figs. 1(e) and 1(f), where points A and B are the $Mg_{17}Al_{12}$ and Mg_2Si phases, respectively. In addition, a large number of SiC particles are uniformly distributed in the α-Mg matrix, as shown in the red rectangular area in Fig. 1(c). After solution treatment, most of the $Mg_{17}Al_{12}$ phases were dissolved into the matrix, whereas the Mg_2Si phases did not disappear. This result is in accordance with the findings of Zhang *et al*. [7]. The Mg–Al binary phase diagram shows that Al exhibited great solid solubility in Mg at 420°C and that the $Mg_{17}Al_{12}$ phases almost disappeared after solution treatment. However, the Mg_2Si phase demonstrated excellent thermal stability and remained in the α-Mg matrix. Fig. 2 shows the XRD patterns of the Mg–9Al–1Si–1SiC alloys. Compared with those of the as-cast sample, the diffraction peaks of $Mg_{17}Al_{12}$ were almost absent in the solution-treated sample. This phenomenon is consistent with the SEM

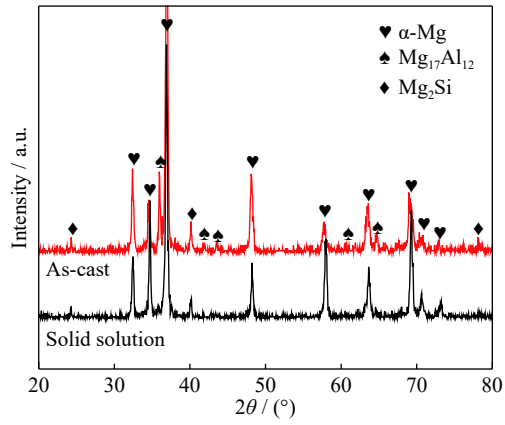

Fig. 2. XRD patterns of as-cast and solution-treated alloys.

and EDS analysis results in Fig. 1. However, the SiC particles were not observed in Fig. 2 because of the less content of SiC nanoparticles.

3.2. Microstructure evolution and texture after ECAP

Fig. 3 displays the optical micrographs and plots of average grain size for the solution-treated alloys processed by multi-pass ECAP at various temperatures. Compared with those of the as-cast alloy, the grains of the processed alloy were refined remarkably by DRX during the ECAP processing, as shown in the red rectangular area in Fig. 3(a). Analysis with Image-Pro Plus software showed that the aver-

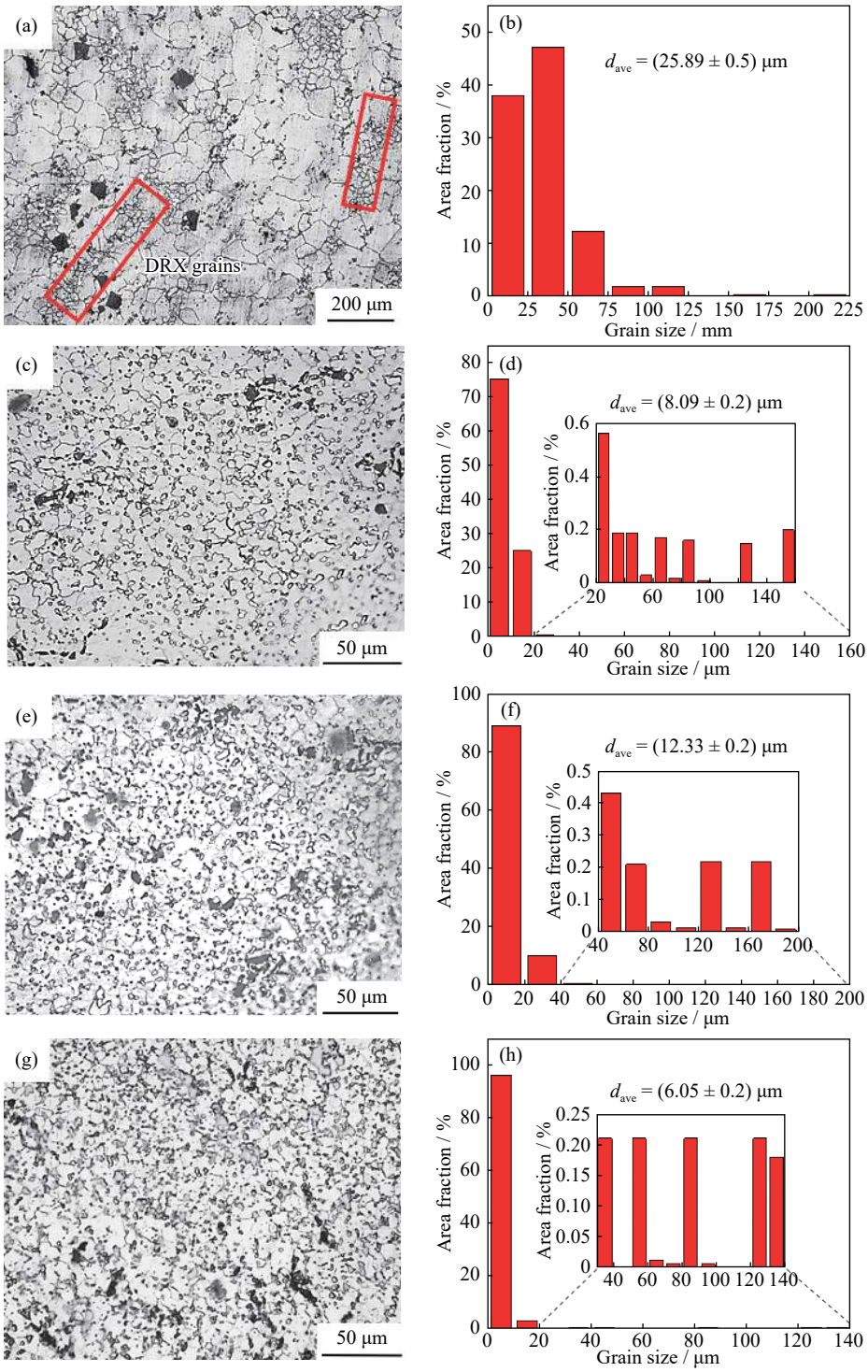

Fig. 3. Optical microstructure images and average grain size plots for samples processed at different ECAP temperatures: (a, b) sample I; (c, d) sample II; (e, f) sample III; (g, h) sample IV.

age grain size of sample I (four ECAP passes at 400°C) was (25.89 ± 0.5) μm. By contrast, the average grain size of sample II (one pass at 400°C, one pass at 360°C, and two passes at 320°C), sample III (one pass at 400°C, two passes at 360°C, and one pass at 320°C), and sample IV (two passes at 400°C and two passes at 320°C) decreased to (8.09 ± 0.2), (12.33 ± 0.2), and (6.05 ± 0.2) μm, respectively. In addition, coarse grains were scarce in samples II, III, and IV. This result indicates that the alloy processed by multi-pass ECAP at various temperatures has finer grains than an alloy processed by conventional ECAP at a constant temperature. The emergence of dynamic recrystallization during the ECAP processing includes two processes of nucleation and growth. The deformation stress level increases with decreasing deformation temperature during hot extrusion, which greatly increases the accumulation of deformation energy and promotes dynamic recrystallization and then further refines the microstructure of the alloy [24]. Meanwhile, low extrusion temperature can suppress grain growth. Similarly, a previous study obtained super-fine gains by reducing the ECAP processing temperature from 300°C to 150°C and allowing the total pass reach eight passes; a much finer microstructure is fabricated by ECAP for eight passes at 300°C [25].

Fig. 4 shows the SEM micrographs of the samples processed by multi-pass ECAP at various temperatures. The extrusion direction (ED) is indicated in Fig. 4(a) with a red arrow. As shown in Fig. 4(a), after four ECAP passes at 400°C, a large number of $Mg_{17}Al_{12}$ precipitation phases appeared along the ED in the matrix, and some Mg_2Si phases still persisted as clusters. Compared with those in sample I, the number of precipitates in samples II, III, and IV increased sharply, and a small number of fine precipitates were obtained in samples II and IV, as shown in the red rectangular area in Figs. 4(b) and 4(d). This result proves that more dispersed and finer precipitation phases can be obtained in the samples processed by four passes of ECAP at various temperatures. In general, the dynamic precipitation phase was induced by the temperature and high strain during the ECAP processing. On the one hand, the strain rapidly accumulated by ECAP processing at low deformation temperatures can provide a high driving force for the dynamic precipitation of the secondary phase. On the other hand, the low extrusion temperature can restrict the re-dissolution of precipitates during the long ECAP inter-pass time (15 min) [26]. Meanwhile, the relatively coarse precipitates (>1 μm) can provide additional sites for grain nucleation through the particle-stimulated nucleation (PSN) mechanism, which can improve the nucleation rate of grains to some extent and contribute to grain refinement. In addition, the fine precipitated particles (<1 μm) can effectively pin grain boundaries and greatly restrain the growth of the recrystallized grains [27], which is consistent with the results in Fig. 3.

Fig. 5 provides a representative TEM micrograph of sample I processed by four ECAP passes at 400°C. As shown in Fig. 5(a), a large number of SiC nanoparticles were distributed at the magnesium matrix, and some high-density dislocation entanglements appeared around the SiC and $Mg_{17}Al_{12}$ particles. The selected area electron diffraction pat-

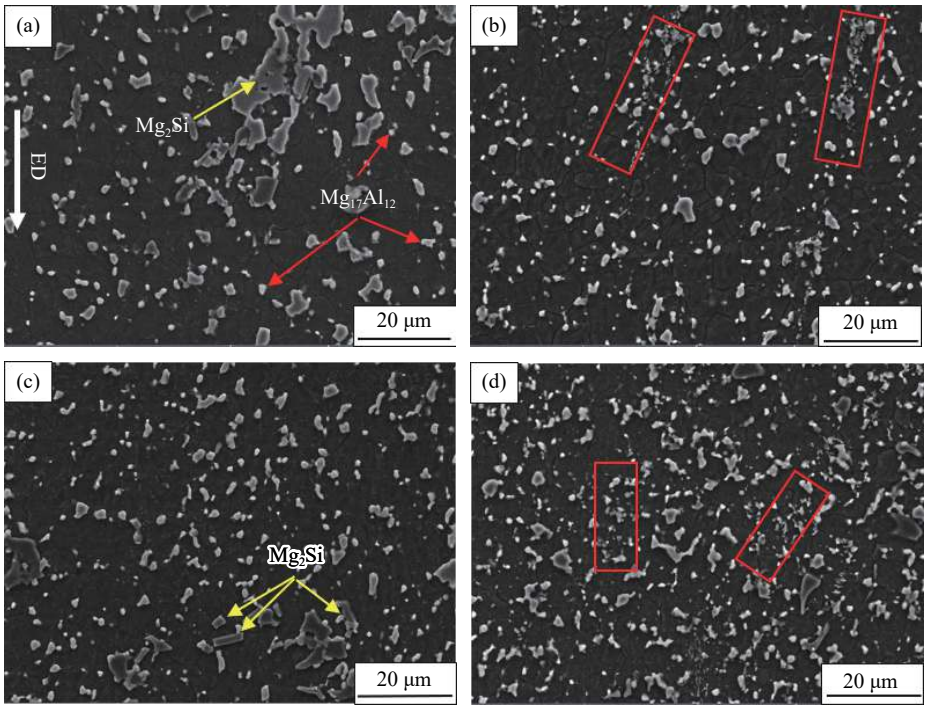

Fig. 4. SEM micrographs of samples processed at different ECAP temperatures: (a) sample I; (b) sample II; (c) sample III; (d) sample IV.

tern in Fig. 5(b) confirms the existence of SiC particles in the matrix. The above description suggests that SiC nanoparticles can pin the dislocation migration, prevent the grain boundary movement, and further promote the dynamic recrystallization and grain refinement of the alloy [28]. Previous studies reported that the SiC nanoparticles and broken Mg_2Si phases can serve as heterogeneous nucleation sites to promote the dynamic precipitation of $Mg_{17}Al_{12}$ during the ECAP processing because of their high surface-to-volume ratio and high surface energy [29]. Meanwhile, broken Mg_2Si particles and dynamic precipitation of $Mg_{17}Al_{12}$ can obviously hinder grain boundary movement and restrain grain growth.

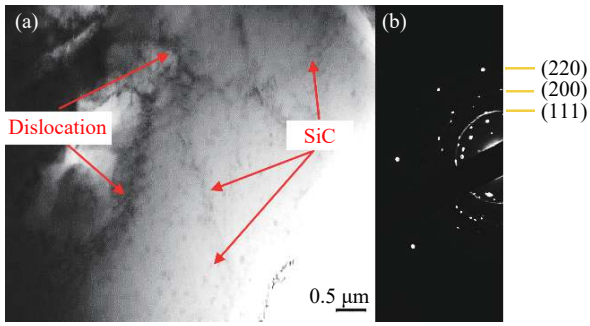

Fig. 5. TEM images of sample I: (a) distribution of dislocations and SiC nanoparticles; (b) electron diffraction of SiC nanoparticles.

Fig. 6 presents the texture evolution of the samples processed by different ECAP processing sequences. As shown in Fig. 6(a), the maximum texture intensity in the (0002) plane was 4.9 MRD (Multiples of random distribution), and the texture showed obvious preference orientation during the ECAP processing. The preferential texture orientation was approximately 60° with respect to the ED. In sample II, the maximum intensity of sample II rotated approximately 30° with respect to the ED, and the maximum texture intensity decreased to 4.0 MRD. However, in sample III, the preferential texture orientation was approximately 45° with away from the ED and the maximum texture intensity increased to 5.8 MRD. By contrast, a random texture can be observed in sample IV, and the intensity of maximum texture further decreased to 3.1 MRD. Previous studies also reported that the maximum texture intensity in the (0002) plane is away from the center of the pole figure during the ECAP processing [22]. The (0002) plane of samples II and IV exhibited weakened texture intensity, which can be related to the completely dynamic recrystallization with a relatively random orientation of the matrix grains [30–31]. In addition, a large number of dynamic precipitates provide randomly oriented nuclei, which is an important factor for obtaining a weakened and randomized texture [7]. Compared with those of samples II and IV, the maximum intensities of samples I and III deviated obviously from the center of the pole figure, which contributed to the sliding of the base plane and improved the ductility of the alloy.

3.3. Mechanical properties

The representative engineering stress–strain curves of the alloys processed with different ECAP temperatures are given in Fig. 7(a), and their mechanical properties at room temperature, specifically ultimate tensile strength (UTS), YS, and elongation to failure (EL), are compared in Fig. 7(b). The strength of the samples processed by ECAP at different temperatures obviously improved when compared with that of sample I. As shown in Fig. 7(b), the YS values of samples II, III, and IV were 194, 175, and 206 MPa, which were higher by 24.4%, 12.2%, and 32.1%, respectively, than the YS in sample I. The UTS also increased to different extents, whereas the elongation decreased except for sample III. On the basis of these microstructure evolutions, the strength increment can be attributed to the grain refinement and dispersed distribution of the $Mg_{17}Al_{12}$ phases because numerous grain boundaries and $Mg_{17}Al_{12}$ phases can effectively pin dislocation motion. However, the elongation of samples II and IV significantly reduced, which may be related to the stress concentration caused by a large volume fraction of $Mg_{17}Al_{12}$ phases and block-shaped Mg_2Si particles at the grain boundaries, which led to premature fracture of the alloy during the tension test.

As described above, two strengthening mechanisms are responsible for the improvement in the mechanical properties of alloys processed by ECAP with various temperature. These mechanisms are the grain boundary strengthening and Orowan strengthening caused by precipitates. The effect of grain boundary strengthening on mechanical properties can be analyzed by the Hall–Petch equation as follows:

$$\sigma_s = \sigma_0 + kd^{-\frac{1}{2}} \tag{1}$$

where σ_s is the YS, σ_0 is a material constant, k is the Hall–Petch coefficient (=130 MPa $\mu m^{1/2}$), and d is the mean grain size [32]. The formula shows that the material strength increases as the grain size decreases. The improvement in YS induced by grain refinement in samples II, III, and IV compared with sample I can be calculated by the following equation:

$$\Delta\sigma_{\text{Hall–Petch}} = k\left(d_X^{-1/2} - d_I^{-1/2}\right) \tag{2}$$

where $\Delta\sigma_{\text{Hall–Petch}}$ is the incremental YS by grain refinement, k is the Hall–Petch coefficient (= 130 MPa $\mu m^{1/2}$), d_I is the average grain size of sample I, and d_X is the average grain size of samples II, III, and IV [33]. With Eq. (2), the improvement in YS induced by grain refinement in samples II, III, and IV was calculated as 20.2, 11.5, and 27.3 MPa, respectively.

However, although fine grains can significantly increase the strength of the alloy, the contribution of Orowan strengthening to YS should not be ignored. As shown in

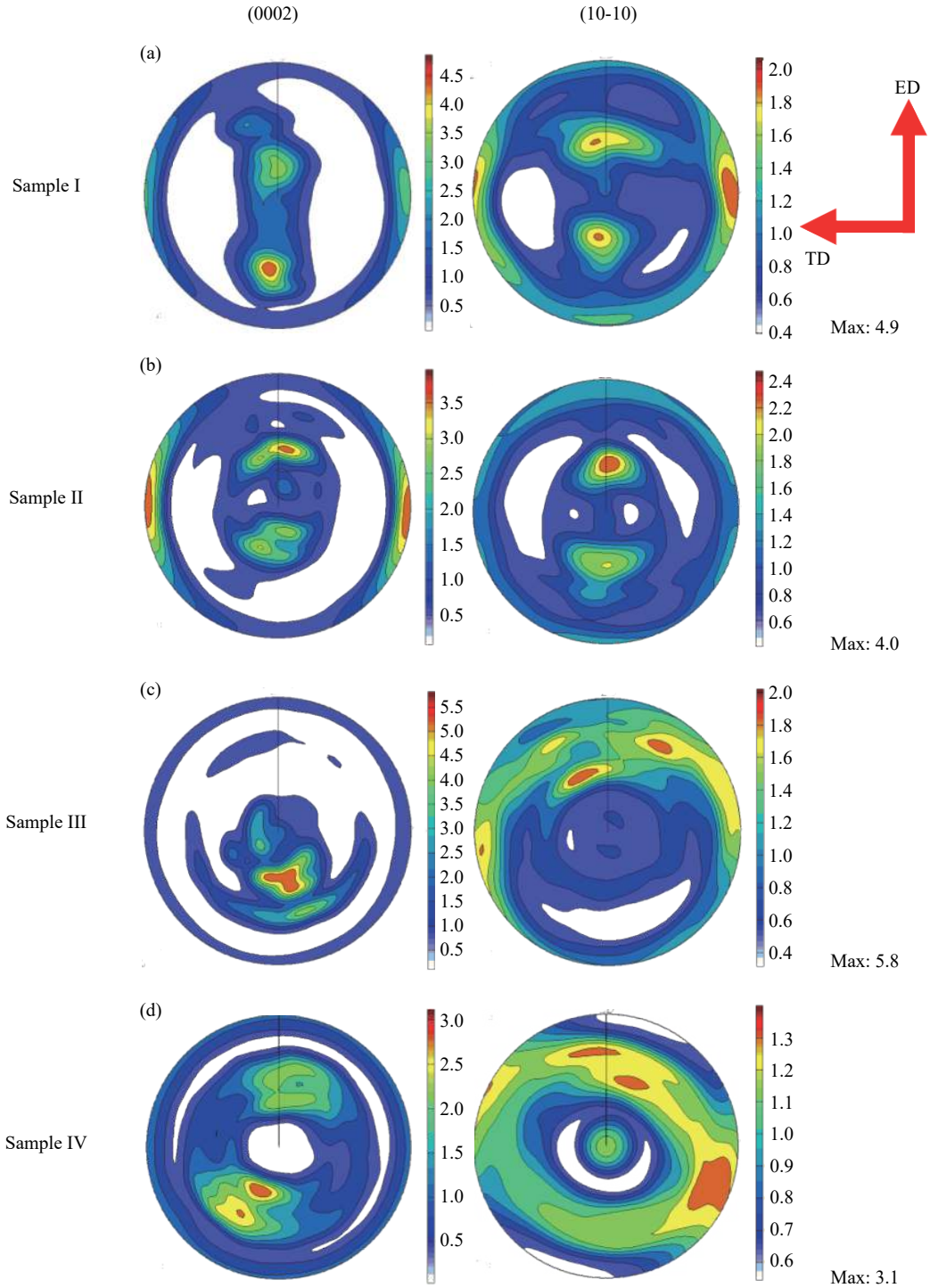

Fig. 6. Global texture of samples processed at different ECAP temperatures: (a) sample I; (b) sample II; (c) sample III; (d) sample IV. ED—Extrusion direction; TD—Transverse direction.

Fig. 4, the volume fractions of precipitates in samples II, III, and IV were higher than that in sample I. In addition, the average precipitate sizes decreased with decreasing extrusion temperature. Meanwhile, the dispersed dynamic precipitates can effectively pin the migration of dislocations, and this strengthening mechanism can be analyzed by the following equation [34]:

$$\Delta\sigma_{\text{Orowan}} = M\frac{0.4Gb}{\pi\sqrt{1-\nu}}\cdot\frac{1}{\bar{d}\left(\sqrt{\frac{\pi}{4f}}-1\right)}\ln\frac{\bar{d}}{b} \tag{3}$$

where M is the strengthening coefficient (1.25), G is the shear modulus of Mg (16.6 GPa), b is the Burgers vector of dislocations (0.32), ν is Poisson's ratio (0.35), $\bar{d}$ is the mean size

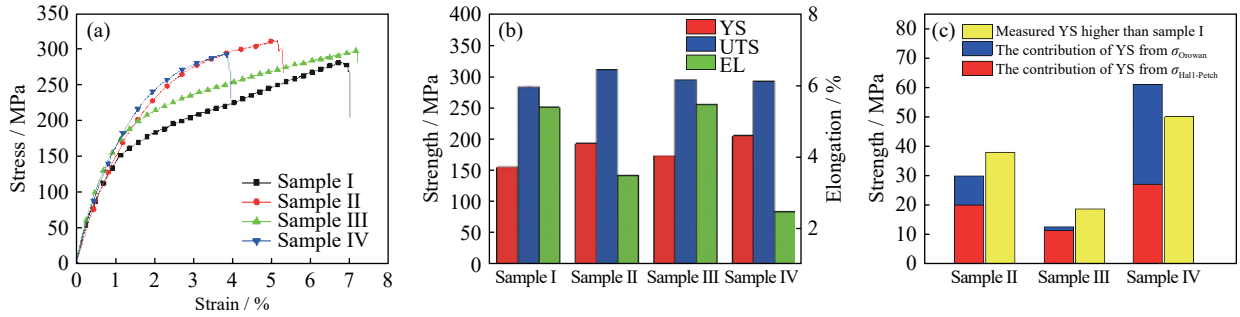

Fig. 7. Tensile properties of samples processed at different ECAP temperatures: (a) tensile stress–strain curves; (b) YS, UTS, and EL; (c) incremental YS induced by grain refinement and dynamic precipitates with respect to sample I.

of precipitates ($=\sqrt{2/3}d_p$), and d_p and f represent the size and volume fraction of precipitates, respectively. On the basis of the above data, the contributions of Orowan strengthening to YS in samples II, III, and IV were higher by 9.7, 1.4, and 33.6 MPa, respectively, than the YS increment in sample I induced by Orowan strengthening. Compared with that in sample I, the YS increment induced by grain refinement and dynamic precipitates is demonstrated in Fig. 7(c). The increment of the theoretical YS in samples II, III, and IV induced by the combination of grain boundary strengthening and Orowan strengthening is basically the same as the actually measured value. These results indicate that grain boundary strengthening is the main mechanism for the increased YS of the composites after multi-pass ECAP at various temperatures and that Orowan strengthening also contributes to the increase in YS.

Fig. 8 shows the SEM micrographs of the tensile fracture surface of the samples. As shown in Fig. 8(a), many tear ridges can be observed, as marked by red arrows, which indicates that sample I failed with a typical plastic fracture. A similar fracture surface was observed in sample III, and a large number of dimples can be observed in Fig. 8(c), which contributed to the ductility of the material. However, a somewhat bulky Mg_2Si phase and cleavage planes can be observed in Figs. 8(b) and 8(d) compared with samples I and III. The large Mg_2Si phase became a crack source and finally failed prematurely during the tension test, which is consistent with the tensile results.

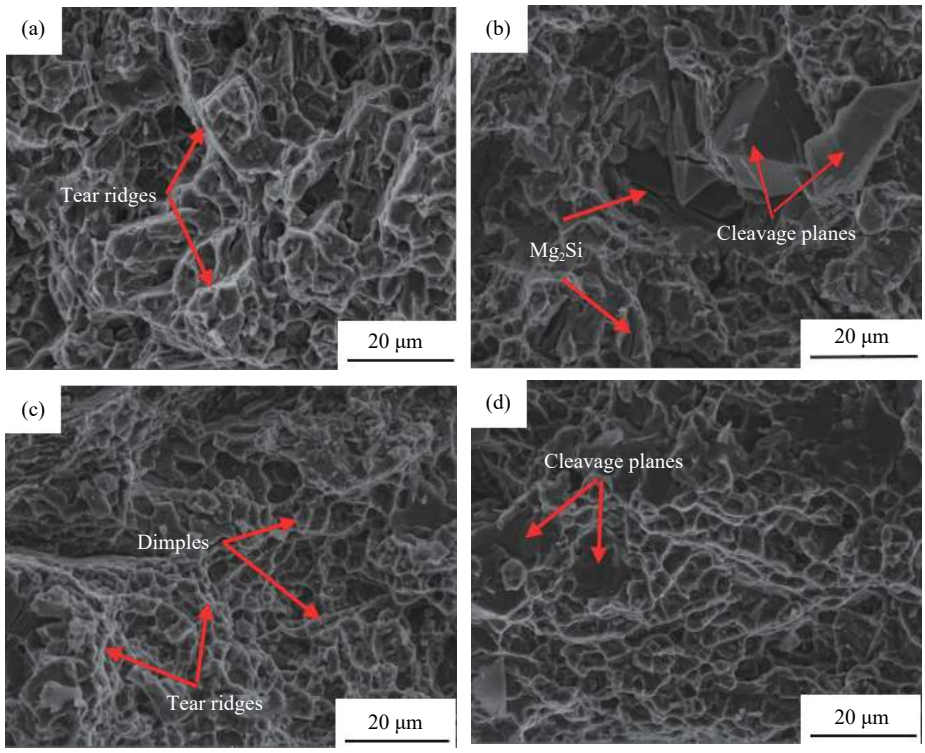

Fig. 8. Fracture surface of room-temperature tensile samples processed at different ECAP temperatures: (a) sample I; (b) sample II; (c) sample III; (d) sample IV.

4. Conclusions

(1) As-cast Mg–9Al–1Si–1SiC alloy was characterized by a dendritic α-Mg matrix, discontinuous $Mg_{17}Al_{12}$ phase, and Chinese script-shaped Mg_2Si phase. Most $Mg_{17}Al_{12}$ phases were dissolved into the α-Mg matrix, whereas Mg_2Si phases remained even after the homogenization treatment at 420°C for 24 h.

(2) The fine grains and dispersed precipitates were obtained in the samples processed by multi-pass ECAP at various temperatures when compared with the samples processed by ECAP at a constant temperature. These features can effectively improve the mechanical properties of the material.

(3) SiC nanoparticles were completely integrated into the matrix by multi-pass ECAP processing, which can effectively pin the dislocations and hinder grain boundary migration. A large number of precipitates can effectively improve the nucleation ratio of recrystallization through a PSN mechanism. The YS improvement of the alloy can be attributed to grain boundary strengthening and Orowan strengthening.

Acknowledgements

This work was supported by the National Natural Science Foundation of China (Nos. 51404166， 51704209, and U1810208), Shanxi province scientific facilities and instruments shared service platform of magnesium-based materials electric impulse aided forming (No. 201805D141005), Science and Technology Major Project of Shanxi province (Nos. 20191102008, 20191102007, 20191102004, and 20181101008), Natural Science Foundation of Shanxi Province (No. 201701D121045), Shanxi Province Science Foundation for Youths (No. 2016021063), and The Projects of International Cooperation in Shanxi (No. 201803D 421086).

References

[1] Y.Z. Lü, Q.D. Wang, X.Q. Zeng, W.J. Ding, C.Q. Zhai, and Y.P. Zhu, Effects of rare earths on the microstructure, properties and fracture behavior of Mg–Al alloys, *Mater. Sci. Eng. A*, 278(2000), No. 1-2, p. 66.

[2] Y. Liu, W. Li, and Y.Y. Li, Microstructure and mechanical properties of ZE10 magnesium alloy prepared by equal channel angular pressing, *Int. J. Miner. Metall. Mater.*, 16(2009), No. 5, p. 559.

[3] H. Mirzadeh, Constitutive behaviors of magnesium and Mg–Zn–Zr alloy during hot deformation, *Mater. Chem. Phys.*, 152(2015), p. 123.

[4] M. Gupta and W.L.E. Wong, Magnesium-based nanocomposites: Lightweight materials of the future, *Mater. Charact.*, 105(2015), p. 30.

[5] D.L. Yu, D.F. Zhang, J. Sun, Y.X. Luo, J.Y. Xu, H.J. Zhang, and F.S. Pan, Improving mechanical properties of ZM61 magnesium alloy by aging before extrusion, *J. Alloys Compd.*, 690(2017), p. 553.

[6] W.H. Wang, H.X. Wang, Y.M. Liu, H.H. Nie, and W.L. Cheng, Effect of SiC nanoparticles addition on the microstructures and mechanical properties of ECAPed Mg9Al–1Si alloy, *J. Mater. Res.*, 32(2017), No. 3, p. 615.

[7] S.X. Zhang, M. Li, H.X. Wang, W.L. Cheng, W.W. Lei, Y.M. Liu, and W. Liang, Microstructure and tensile properties of ECAPed Mg–9Al–1Si–1SiC composites: The influence of initial microstructures, *Materials*, 11(2018), No. 1, art. No. 136.

[8] K.B. Nie, K.K. Deng, X.J. Wang, W.M. Gan, F.J. Xu, K. Wu, and M.Y. Zheng, Microstructures and mechanical properties of SiC_p/AZ91 magnesium matrix nanocomposites processed by multidirectional forging, *J. Alloys Compd.*, 622(2015), p. 1018.

[9] X.G. Qiao, T. Ying, M.Y. Zheng, E.D. Wei, K. Wu, X.S. Hu, W.M. Gan, H.G. Brokmeier, and I.S. Golovin, Microstructure evolution and mechanical properties of nano-SiC_p/AZ91 composite processed by extrusion and equal channel angular pressing (ECAP), *Mater. Charact.*, 121(2016), p. 222.

[10] K.B. Nie, X.J. Wang, X.S. Hu, L. Xu, K. Wu, and M.Y. Zheng, Microstructure and mechanical properties of SiC nanoparticles reinforced magnesium matrix composites fabricated by ultrasonic vibration, *Mater. Sci. Eng. A*, 528(2011), No. 15, p. 5278.

[11] K.B. Nie, X.J. Wang, L. Xu, K. Wu, X.S. Hu, and M.Y. Zheng, Influence of extrusion temperature and process parameter on microstructures and tensile properties of a particulate reinforced magnesium matrix nanocomposite, *Mater. Des.*, 36(2012), p. 199.

[12] K.B. Nie, X.J. Wang, X.S. Hu, Y.W. Wu, K.K. Deng, K. Wu, and M.Y. Zheng, Effect of multidirectional forging on microstructures and tensile properties of a particulate reinforced magnesium matrix composite, *Mater. Sci. Eng. A*, 528(2011), No. 24, p. 7133.

[13] K.B. Nie, X.J. Wang, K. Wu, L. Xu, M.Y. Zheng, and X.S. Hu, Processing, microstructure and mechanical properties of magnesium matrix nanocomposites fabricated by semisolid stirring assisted ultrasonic vibration, *J. Alloys Compd.*, 509(2011), No. 35, p. 8664.

[14] R.Z. Valiev and T.G. Langdon, Principles of equal-channel angular pressing as a processing tool for grain refinement, *Prog. Mater. Sci.*, 51(2006), No. 7, p. 881.

[15] J. Wei, G.H. Huang, D.D. Yin, K.N. Li, Q.D. Wang, and H. Zhou, Effects of ECAP and annealing treatment on the microstructure and mechanical properties of Mg–1Y (wt. %) binary alloy, *Metals*, 7(2017), No. 4, art. No. 119.

[16] M.Y. Zheng, X.G. Qiao, S.W. Xu, K. Wu, S. Kamado, and Y. Kojima, *In-situ* quasicrystal-reinforced magnesium matrix composite processed by equal channel angular extrusion (ECAE), *J. Mater. Sci.*, 40(2005), No. 9-10, p. 2587.

[17] J. Suh, J. Victoria-Hernández, D. Letzig, R. Golle, and W. Volk, Effect of processing route on texture and cold formability of AZ31 Mg alloy sheets processed by ECAP, *Mater. Sci. Eng. A*, 669(2016), p. 159.

[18] M. Bleckmann, M. Eichhorst, M. Schuch, W. Kreuzer, V.H. Hammond, C. Spiller, L.W. Meyer, and N. Herzig, The influence of selected ECAP-processing routes on the material properties of Magnesium Elektron 675, *Mater. Sci. Eng. A*, 660(2016), p. 108.

[19] H. Liu, H. Huang, X.W. Yang, C. Li, J.L. Yan, J.H. Jiang, and A.B. Ma, Microstructure and mechanical property of a high-strength Mg–10Gd–6Y–1.5Zn–0.5Zr alloy prepared by multi-pass equal channel angular pressing, *J. Magnesium Alloys*, 5(2017), No. 2, p. 231.

[20] H. Liu, Z.J. Cheng, K. Yan, J.L. Yan, J. Bai, J.H. Jiang, and A.B. Ma, Effect of multi-pass equal channel angular pressing on the microstructure and mechanical properties of a heterogeneous $Mg_{88}Y_8Zn_4$ alloy, *J. Mater. Sci. Technol.*, 32(2016), No. 12, p. 1274.

[21] Z.Q. Yang, A.B. Ma, H. Liu, D. Song, Y.N. Wu, Y.C. Yuan, J.H. Jiang, and J.P. Sun, Managing strength and ductility in AZ91 magnesium alloy through ECAP combined with prior and post aging treatment, *Mater. Charact.*, 152(2019), p. 213.

[22] W.J. Kim, S.I. Hong, Y.S. Kim, S.H. Min, H.T. Jeong, and J.D. Lee, Texture development and its effect on mechanical properties of an AZ61 Mg alloy fabricated by equal channel angular pressing, *Acta Mater.*, 51(2003), No. 11, p. 3293.

[23] D. Orlov, G. Raab, T.T. Lamark, M. Popov, and Y. Estrin, Improvement of mechanical properties of magnesium alloy ZK60 by integrated extrusion and equal channel angular pressing, *Acta Mater.*, 59(2011), No. 1, p. 375.

[24] Y.C. Lin and X.M. Chen, A critical review of experimental results and constitutive descriptions for metals and alloys in hot working, *Mater. Des.*, 32(2011), No. 4, p. 1733.

[25] Y.C. Yuan, A.B. Ma, X.F. Gou, J.H. Jiang, G. Arhin, D. Song, and H. Liu, Effect of heat treatment and deformation temperature on the mechanical properties of ECAP processed ZK60 magnesium alloy, *Mater. Sci. Eng. A*, 677(2016), p. 125.

[26] T. Yuan, J.H. Jiang, A.B. Ma, Y.N. Wu, Y.C. Yuan, and C. Li, Simultaneously improving the strength and ductility of an Al–5.5Mg–1.6Li–0.1Zr alloy via warm multi-pass ECAP, *Mater. Charact.*, 151(2019), p. 530.

[27] J.D. Robson, D.T. Henry, and B. Davis, Particle effects on recrystallization in magnesium-manganese alloys: Particle-stimulated nucleation, *Acta Mater.*, 57(2009), No. 9, p. 2739.

[28] X. Yao, Y.F. Zheng, M.Z. Quadir, C. Kong, J.M. Liang, Y.H. Chen, P. Munroe, and D.L. Zhang, Grain growth and recrystallization behaviors of an ultrafine grained Al–0.6wt%Mg–0.4wt%Si–5vol.%SiC nanocomposite during heat treatment and extrusion, *J. Alloys Compd.*, 745(2018), p. 519.

[29] Z.W. Wang, M. Song, C. Sun, and Y.H. He, Effects of particle size and distribution on the mechanical properties of SiC reinforced Al–Cu alloy composites, *Mater. Sci. Eng. A*, 528(2011), No. 3, p. 1131.

[30] M.G. Jiang, H. Yan, and R.S. Chen, Twinning, recrystallization and texture development during multi-directional impact forging in an AZ61 Mg alloy, *J. Alloys Compd.*, 650(2015), p. 399.

[31] Y.F. Chai, B. Jiang, J.F. Song, Q.H. Wang, J.J. He, J. Zhao, G.S. Huang, Z.T. Jiang, and F.S. Pan, Role of Al content on the microstructure, texture and mechanical properties of Mg–3.5Ca based alloys, *Mater. Sci. Eng. A*, 730(2018), p. 303.

[32] Z. Yang, J.P. Li, Y.C. Guo, T. Liu, F. Xia, Z.W. Zeng, and M.X. Liang, Precipitation process and effect on mechanical properties of Mg–9Gd–3Y–0.6Zn–0.5Zr alloy, *Mater. Sci. Eng. A*, 454(2007), p. 274.

[33] K.K. Deng, J.Y. Shi, C.J. Wang, X.J. Wang, Y.W. Wu, K.B. Nie, and K. Wu, Microstructure and strengthening mechanism of bimodal size particle reinforced magnesium matrix composite, *Compos. Part A*, 43(2012), No. 8, p. 1280.

[34] W.L. Cheng, Q.W. Tian, H. Yu, H. Zhang, and B.S. You, Strengthening mechanisms of indirect-extruded Mg–Sn based alloys at room temperature, *J. Magnesiun Alloys*, 2(2014), No. 4, p. 299.